JOURNAL OF MATERIALS SCIENCE 14 (1979) 2074–2082

The defect structure of MgO containing trivalent cation solutes: the oxidation-reduction behaviour of iron

W. H. GOURDIN*, W. D. KINGERY, J. DRIEAR
Ceramics Division, Department of Materials Science and Engineering, Massachusetts Institute of Technology, Cambridge, Massachusetts 02139, USA

Association energies for ferric ion magnesium vacancy dimers and trimers derived from shell-model calculations are combined with oxidation–reduction equilibria data in concentrated crystalline solutions to derive equilibrium defect concentrations for relatively dilute solutions. The several simultaneous non-linear equations required are solved with a numerical iteration method. Calculated results are compared with experimental determinations of solute concentration and oxygen pressure. It is found that with a slight reduction of the shell-model energies, the defect model is in good accord with experimental data at temperatures greater than 1300° C. At lower temperatures, agreement is poor and it is surmised that solute–vacancy clusters may be important.

1. Introduction

Various plausible point defect configurations involving vacancies and trivalent cation solutes in magnesia have recently been investigated theoretically using the Harwell Automatic Defect Evaluation System (HADES) program [1]. Those calculations suggest a solution model consisting of a hierarchy of cation vacancy – cation solute dimers, trimers and clusters which is in qualitative agreement with the limited data available. In this paper we propose to define a mass-action defect model in terms of the concentration of species present as a function of temperature, solute content and oxygen partial pressure and to develop a numerical calculation method for solving the several non-linear simultaneous equations required. Experimental studies of the oxidation–reduction behaviour of iron as a solute in MgO single crystals are then reported which allow a qualitative corroboration of the model behaviour as well as an evaluation of defect association energies.

2. Oxidation–reduction of iron in MgO: the defect model

One can imagine the dissolution of both the ferrous and ferric ions† in MgO:

$$FeO \overset{MgO}{\rightarrow} Fe_{Mg}^{x} + O_{0}^{x} \quad \Delta G_1^\circ \qquad (1)$$

$$Fe_2O_3 \overset{MgO}{\rightarrow} (Fe_2O_3)_{ss} \quad \Delta G_2^\circ. \qquad (2)$$

Since wüstite can be oxidized to form hematite,

$$2FeO + \tfrac{1}{2}O_2 \rightleftarrows Fe_2O_3 \quad \Delta G_3^\circ \qquad (3)$$

one may combine Reactions 1 to 3 to obtain the oxidation–reduction process in solid solution:

$$2O_0^x + 2Fe_{Mg}^x + \tfrac{1}{2}O_2 \overset{MgO}{\rightleftarrows} (Fe_2O_3)_{ss}$$

$$\Delta G_4^\circ = \Delta G_3^\circ + \Delta G_2^\circ - 2\Delta G_1^\circ. \qquad (4)$$

There are a variety of ways in which the hematite can go into solution. At one extreme, which will occur for very low concentrations of solute, all the iron will be unassociated, and Reaction 4 may be written as

$$2Fe_{Mg}^x + \tfrac{1}{2}O_2 \overset{MgO}{\rightleftarrows} 2Fe_{Mg}^{\cdot} + O_0^x + V_{Mg}'' \quad \Delta G_5^\circ, \qquad (5)$$

*Presently with the Western Electric Engineering Research Center, P.O. Box 900, Princeton, New Jersey 08540, USA.

†These are the only oxidation states obtained under the conditions of this study (Fe^+ may be formed in irradiated specimens [1]).

0022–2461/79/092074–09 $02.90/0

for which the mass-action equilibrium expression is

$$\frac{[Fe_{Mg}^{\cdot}]^2\,[V_{Mg}'']}{[Fe_{Mg}^{x}]^2\,P_{O_2}^{1/2}} = K_5 = \exp\left(-\frac{\Delta G_5^{\circ}}{kT}\right), \quad (6)$$

where the O_0^x activity has been taken to be unity and the brackets indicate site fraction. If iron is the predominant solute, then from the electroneutrality condition, $\frac{1}{2}[Fe_{Mg}^{\cdot}] = [V_{Mg}'']$ and Equation 6 becomes

$$\frac{[Fe_{Mg}^{\cdot}]^3}{[Fe_{Mg}^{x}]^2\,P_{O_2}^{1/2}} = 2K_5 = K_5'. \quad (7)$$

As the amount of iron in solution is increased, or the temperature is lowered, clusters of ferric ions and vacancies are expected to form. Restricting the discussion to high temperatures, the number of large clusters will be small and it is reasonable to assume the principal cluster groupings to be dimers and trimers. Ignoring the distinction between the ⟨1 1 0⟩ and ⟨1 0 0⟩ orientations and linear and non-linear trimers, at the alternative extreme all the ferric ions are bound into neutral trimers so that the solution process may be written:

$$2Fe_{Mg}^{x} + \tfrac{1}{2}O_2 \overset{MgO}{\rightleftarrows} (Fe_{Mg}^{\cdot} - V_{Mg}'' - Fe_{Mg}^{\cdot})^x + O_0^x \quad \Delta G_8^{\circ}, \quad (8)$$

for which

$$\frac{[(Fe_{Mg}^{\cdot} - V_{Mg}'' - Fe_{Mg}^{\cdot})^x]}{[Fe_{Mg}^{x}]^2\,P_{O_2}^{1/2}} = K_8 = \exp\left(-\frac{\Delta G_8^{\circ}}{kT}\right), \quad (9)$$

Since $[Fe^{3+}] = 2[(Fe\text{–}V\text{–}Fe)^x]$, Equation 9 becomes*

$$\frac{[Fe^{3+}]}{[Fe_{Mg}^{x}]^2\,P_{O_2}^{1/2}} = 2K_8 = K'. \quad (10)$$

Between these two extremes, of course, one has a "mixed mode" solution process involving dimers, trimers and unassociated solute ions in varying proportions.

Brynestad and Flood [2] were apparently the first to specifically consider the oxidation–reduction process in magnesiowüstite. They studied the variation of the ratio $R = [Fe^{3+}]/[Fe]_T$, where $[Fe]_T$ is the total iron concentration, in polycrystalline samples of magnesiowüstite heat-treated at 1400° C in various partial pressures of oxygen. Specimens were quenched and analysed for both $[Fe^{2+}]$ and $[Fe]_T$ using wet chemical titration techniques. The reliance on wet chemistry restricted the composition range to $X_{Mg} \leqslant 0.98$ where X_i is the cation fraction.† The striking feature of their results is the decrease in R as the iron content decreases (X_{Mg} increases), which is consistent with the redox process [8]; Brynestad and Flood found that their data could be adequately described by assuming all the ferric ions to be associated into neutral trimers. Speidel [3] and Katsura and Kimura [4] performed similar studies at 1300 and 1160° C, respectively. Soong and Cutler [5] determined R at various temperatures and oxygen isobars using thermogravimetric techniques. From these data in the range 2 to 10% Fe, the equilibrium constant K' has been calculated from Equation 10 and is plotted as Fig. 1 to obtain

$$\ln K' = \frac{25\,600}{T} - 7.66, \quad (11)$$

from which,

$$\Delta G_8^{\circ} = -50\,842 + 16.59T \text{ cal} = -2.20 + (7.20 \times 10^{-4})T \text{ eV}. \quad (12)$$

In a more recent study, for iron contents greater than 3% and the temperature range 900 to 1500° C, Valet *et al.* [6] concluded that their data were consistent with Brynestad and Flood, obtaining [6, 7],

$$\Delta G_8^{\circ} = -2.13 + (7.05 \times 10^{-4})T \text{ eV}, \quad (13)$$

in excellent accord with previous data. Thermogravimetric studies by Reijnen [8] are in good accord with concentration and temperature dependence of other data, but the pre-exponential term is widely different.

Thus, data for systems containing more than about 2% iron show that the ratio $R = [Fe^{3+}]/[Fe]_T$ (1) decreases as $[Fe]_T$ decreases, (2) increases with increasing P_{O_2}, and (3) decreases

*Here $[Fe^{3+}]$ is the total site fraction of ferric iron. This is to be distinguished from $[Fe_{Mg}^{\cdot}]$, the concentration of unassociated Fe^{3+}. For Equation 5, $[Fe^{3+}] = [Fe_{Mg}^{\cdot}]$.

†Defined as $X_{Mg} = n_{Mg}^{2+}/(n_{Mg}^{2+} + n_{Fe}^{2+} + n_{Fe}^{3+})$ where n is the number of the respective ions present. The cation fraction, X_i, is to be distinguished from the site fraction, represented by square brackets, although for $X_i \leqslant 0.02$ the difference between the two is very small.

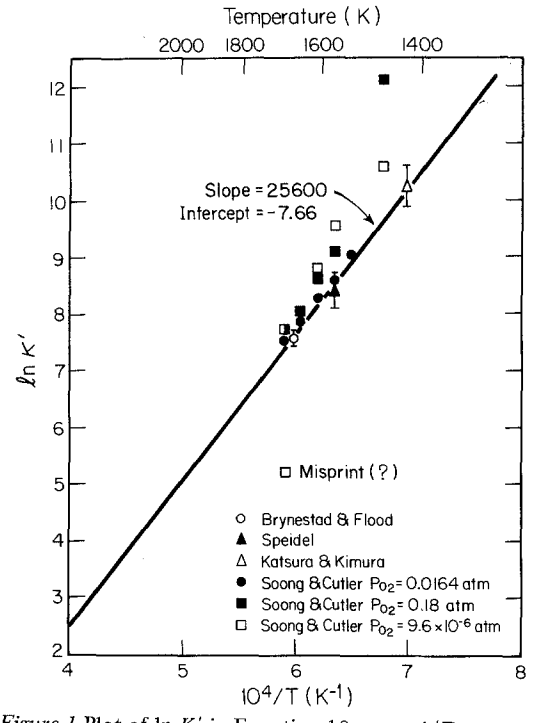

Figure 1 Plot of ln K' in Equation 10 versus $1/T$.

with increasing T at fixed P_{O_2}. Over the concentration range 2 to 10% Fe, the data are consistent with the model of Equation 10 with ΔG° given by Equation 12. Because of Debeye–Hückle effects, solute–solute interactions and indistinguishability of simple associates, it is surprising that such a simple model describes the data so well.

While Equation 10 predicts and experiments show a decreasing value of the ratio $R = [Fe^{3+}]/[Fe]_T$ as $[Fe]_T$ decreases, Equation 7 which is applicable to low concentrations predicts the opposite. Calculation of R as a function of $[Fe]_T$, using reasonable estimates [1] for the energies and pre-exponentials, indicates that a minimum should occur in the concentration range 1000 to 3000 ppm site fraction Fe. This consequence of the model is subject to experimental test.

3. Defect model calculations

To calculate the concentration of defect species present, mass-action equilibrium relations are written for each of the species present, considering the dimer and trimer orientations in the ⟨1 1 0⟩ and ⟨1 0 0⟩ directions, i.e. $(Fe_{Mg}^{\cdot}-O-V_{Mg}'')'(\langle 1\,0\,0\rangle)$, $(Fe_{Mg}^{\cdot}-V_{Mg}'')'(\langle 1\,1\,0\rangle)$, $(Fe_{Mg}^{\cdot}-O-V_{Mg}''-O-Fe_{Mg}^{\cdot})^x(\langle 1\,0\,0\rangle)$ and $(Fe_{Mg}^{\cdot}-V_{Mg}''-Fe_{Mg}^{\cdot})^x(\langle 1\,1\,0\rangle)$, as individual species along with $Fe_{Mg}^{\cdot}$, V_{Mg}'', and $V_O^{\cdot\cdot}$. Aluminium and chromium are present in small amounts and in the present work have been treated collectively, although they could be evaluated separately. Equations are written for the formation of each defect associate with an appropriate pre-exponential entropy and energy term for each reaction process. These equilibrium expressions are combined with (1) a conservation of charge equation providing for electrical neutrality, (2) a site conservation equation providing for the same number of cation and anion sites, and (3) mass conservation equations for each of the solutes present in the system. This provides a system of non-linear simultaneous equations which are solved numerically, using Newton–Raphson iteration [9] in multiple dimensions, for the concentration of each defect as a function of sample composition, temperature and oxygen partial pressure.

4. Experimental details

Samples of MgO single crystals containing less than 1% Fe were annealed at 1200 to 1600° C in different oxygen pressures and quenched. Using optical absorption spectroscopy and neutron activation analysis, the ratio $R = [Fe^{+3}]/[Fe]_T$ was determined and compared with the defect models already described.

4.1. Specimen characterization and heat treatment

Samples from the Norton Co. (NOR), W. C. Spicer Ltd, (SP) and Oak Ridge National Laboratory (ORNL) were analysed by neutron activation analysis and emission spectroscopy as shown in Table I. For reasons not known at present, the Oak Ridge sample was found to have oxidation–reduction kinetics more than a hundred times slower than the other samples. As a result, attainment of equilibrium is suspect in some cases and data for this sample were not used for subsequent analyses. (Study of the kinetics is in progress.)

Specimens were carefully thinned, and the final polish was achieved with colloidal silica (Monsanto Co. "Syton"). Only a few surface flaws were visible at × 320 magnification. Sample thickness ranged from 0.0366 cm (NOR 1–122) to 1.21 × 10^{-3} cm (SP 1–8500).

Samples were annealed in an atmosphere of argon–oxygen or CO–CO_2 in a molybdenum-wound verticle tube furnace controlled to ± 5° C. The P_{O_2} was measured directly with a ZrO_2 cell operating at 800° C. While existing studies [7, 10–

TABLE I Sample analyses

(a) Neutron activation analysis*

Sample	Fe		Cr		Mn	
	Wt fraction	Cation fraction (ppm)	Wt fraction	Cation fraction (ppm)	Wt fraction	Cation fraction (ppm)
NOR1–122	$1.54 \pm 0.09 \times 10^{-4}$	111 ± 7	$70 \pm 1.4 \times 10^{-7}$	0.5 ± 0.1	$< 7 \times 10^{-6}$	< 5
SP1–310	$4.60 \pm 0.32 \times 10^{-4}$	332 ± 23	$2.4 \pm 0.5 \times 10^{-5}$	19 ± 4	$5.6 \pm 1.7 \times 10^{-5}$	41 ± 12
SP1–2300	$4.49 \pm 0.27 \times 10^{-3}$	3247 ± 195	$2.7 \pm 0.5 \times 10^{-6}$	2.1 ± 0.4	$< 2.7 \times 10^{-5}$	< 20
SP1–4300	$6.38 \pm 0.38 \times 10^{-3}$	4615 ± 277	$3.5 \pm 0.7 \times 10^{-6}$	2.8 ± 0.6	$< 1.8 \times 10^{-5}$	< 13
SP1–8500	$1.02 \pm 0.04 \times 10^{-2}$	7365 ± 295	$4.4 \pm 0.9 \times 10^{-6}$	3.4 ± 0.7	Not detected	Not detected
ORNL1–65	$9.68 \pm 0.97 \times 10^{-5}$	70 ± 7	$1.4 \pm 0.3 \times 10^{-5}$	11 ± 2	$< 1.5 \times 10^{-5}$	< 11

*Performed by General Electric Company, Vallecitos Nuclear Center, Pleasanton, California, USA. Precision is within ± 10%.

(b) Quantitative emission spectroscopy†

Sample	Al		Ca		Si		Misc cations (ppm)
	Wt fraction	Cation fraction (ppm)	Wt fraction	Cation fraction (ppm)	Wt fraction	Cation fraction (ppm)	
NOR1–122	2×10^{-5}	30	1.2×10^{-4}	121	3×10^{-5}	43	Ag < 0.4 Cu < 4 Ti < 8
SP1–310	7×10^{-6}	11	7×10^{-5}	70	2×10^{-5}	29	Ag < 0.4 Cu < 6
SP1–2300	2×10^{-6}	3	1.4×10^{-5}	14	2×10^{-6}	3	–
SP1–4300	$< 10^{-6}$	< 1.5	5×10^{-6}	5	2×10^{-6}	3	–
SP1–8500	$< 10^{-6}$	< 1.5	3×10^{-6}	3	2×10^{-6}	3	–
ORNL1–65	4×10^{-5}	60	7×10^{-5}	70	2×10^{-5}	29	Ag < 0.4 Cu < 4 Ti < 8

†Performed by W. Correia, MIT, USA. Error in the values is ± 30% or more.

13] do not completely clarify details of the redox process, they provide data for the time for a slab to reach equilibrium (an effective diffusion coefficient) which are in accord with our observations. Annealing time ranged from 15 min for the thin samples at 1500 and 1600° C to 300 min for the thick samples at 1200 and 1300° C.

Quenching was achieved by vaporizing a platinum support wire and allowing the samples to free fall out of the furnace in a stream of upward-flowing gas. Since the thermal equilibration time for a thin sample is of the order of 10^{-4} sec, the quench rate is determined by the time-of-fall, about 0.17 sec to 600° C, which is a very small fraction of the redox equilibration time. However, atomic rearrangements over many angstroms (such as trimer/dimer re-orientation or cluster formation) may well occur, as might electronic transitions. Based on simple models for the energy level structure of iron in solid solution in MgO [14–16], a crude calculation [7] indicates that electronic rearrangements at temperatures as high as 1600° C are negligible.

Calibration of the optical absorption data necessitated the reliable chemical determination of $[Fe^{3+}]$ and $[Fe]_T$ for one sample. For this purpose, a large sample of MgO containing 1 wt % iron ($[Fe]_T \approx 7365$ ppm) was prepared by co-precipitation of the hydroxides. The resulting powder was pressed into pellets, packed in powder of the same composition and fired at 1700° C. X-ray diffraction confirmed that the specimens were single-phase MgO. These pellets were heat-treated for 65 h in oxygen at 1400° C, quenched and analysed for $[Fe^{2+}]$ and $[Fe]_T$ after dissolving in HCl under an atmosphere of CO_2. At 1400° C and $P_{O_2} = 1$ atm, it was found for this sample that $R_0 = [Fe^{3+}]_0/[Fe]_T = 0.80 \pm 0.01$.

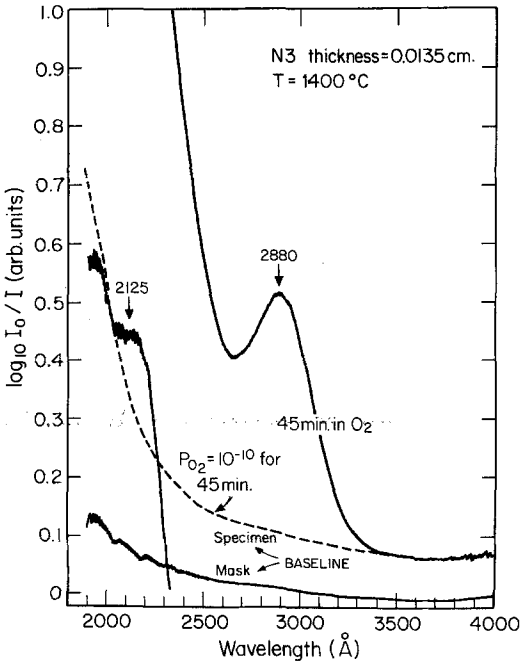

Figure 2 Typical absorption spectrum showing specimen baseline. The peak at 2125 Å has been displaced down 1.0 units.

4.2. Optical absorption measurements

The characteristic ultraviolet absorption at 5.7 and 4.3 eV (2150 and 2880 Å) has been much studied [10, 14, 15, 17–19] and proposed by Chen and Sibley [17] and Davidge [11] as a method of determining ferric iron content. Typical absorption curves are shown in Fig. 2. Measurements were made with a Cary 14 spectrometer, introducing appropriate corrections for surface reflectivity to obtain the absorption coefficient at 2880 Å.

In Fig. 3, Davidge's [11] results for samples equilibrated in air and Chen and Sibley's [17] results for samples saturated under γ irradiation, as well as data from this study for samples equilibrated in oxygen at 1400° C are collected.

From the linearity of Fig. 3 and chemical analyses for $[\mathrm{Fe}]_T \approx 7365$ ppm it follows that $R_0 \approx 0.80$ for all samples saturated in an oxygen atmosphere at 1400° C. Under general conditions of temperature, composition and oxygen partial pressure, R may be determined as

$$R = [\mathrm{Fe}^{3+}]/[\mathrm{Fe}]_T = R_0(\alpha/\alpha_0)$$

where α_0 is the saturation absorption at 2880 Å. (Davidge [11] calculated an oscillator strength of 0.04 assuming that $R = 1$ in air, this should be ≈ 0.05 based on our chemical analysis.) Davidge [11] suggested that the 4.3 eV absorption might be due to unassociated ferric ions. However, calculations [20] indicate that it is the first coordination shell of oxygen ions which determine the charge transfer spectrum. Furthermore, the variation of heat-treatments and, therefore, of the ratio of unassociated ions is large for the samples shown in Fig. 3. Thus, both theory and experiment support the use of the absorption coefficient as a measure of the total ferric ion content.

5. Results and discussion

Starting with the association energies calculated by Gourdin and Kingery [1] and the experimental value (discussed in Section 2) of the standard free-energy change of the redox reaction in which

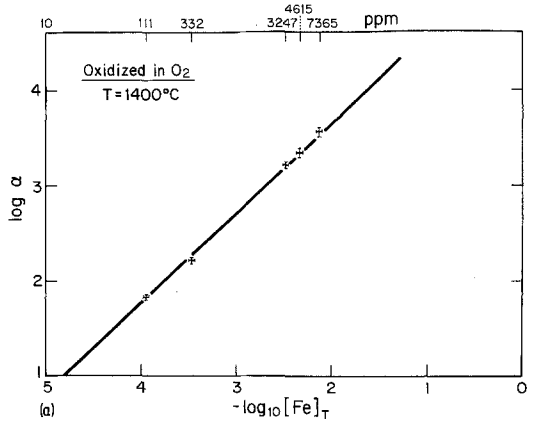

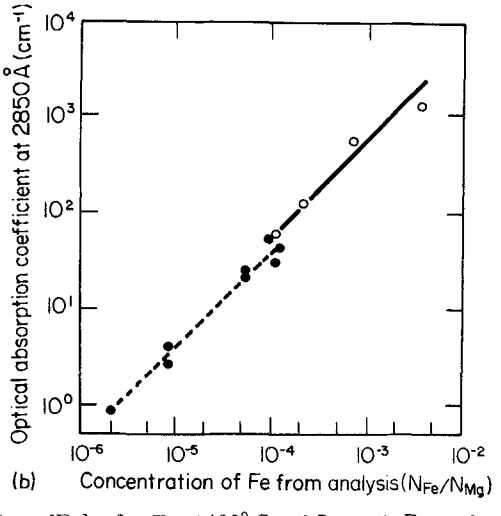

Figure 3 (a) Calibration curve of $\log_{10}\alpha(\lambda = 2880\ \text{Å})$ versus $\log_{10}[\mathrm{Fe}]_T$ for $T = 1400°$ C and $P_{O_2} = 1$. From the plot, $\log_{10}\alpha = \log_{10}[\mathrm{Fe}]_T + 5.686$. (b) Data of Chen and Sibley [17] (dashed line) and Davidge [11] (solid line) for the absorption coefficient at ~ 2880 Å as a function of [Fe].

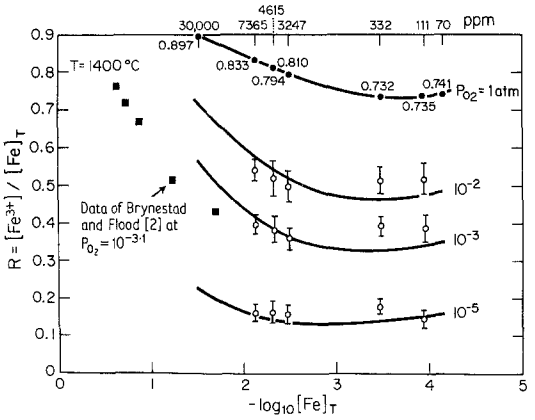

Figure 4 Plot of R values calculated at $T = 1400°$ C for various partial pressures of oxygen using energies of association as calculated from the shell model. See Table II.

the Fe^{3+} is fully associated, and taking the pre-exponentials for the association process to consist only of configurational terms, the free-energy change for the unassociated redox, Equation 5, can be deduced. The ratios R_0 and R may then be calculated for comparison with experiment. As shown in Fig. 4, the comparison with experimental data is not too bad, but the R_0 values (which should be approximately constant) vary from 0.74 to 0.83, the curves do not connect well with data of Brynestad and Flood [2], and experimental values are higher than those calculated at the intermediate oxygen pressures and lower iron contents. This result is not surprising since Gourdin and Kingery [1] indicated for other reasons that the calculated energy values were somewhat too large.

Scaled down values of the associate binding energies were tested for internal consistency and agreement with the experimental data. Because of the complexity of the defect model involving sums of exponentials, a "best fit" to the data in a statistical sense would be very difficult, at best, and no attempt was made at any sophisticated statistical analysis. Data were fitted by trial and error, and the results do not necessarily provide a unique set of parameters able to describe the system behaviour.

Using configurational pre-exponential terms, constants which are in accord with the experimental results are collected in Table II. Taking the absorption coefficient of samples at $P_{O_2} = 1$ as unity, the relative change of Fe^{+3} concentration as a function of log P_{O_2} is nearly linear and in excellent agreement with the experimental data as shown for two samples in Fig. 5. Assuming that ⟨1 0 0⟩ trimers predominate, we calculate

$$\Delta G_8^0 = -2.12 + 7.85 \times 10^{-4}\, T\text{eV}, \quad (14)$$

in fair accord with Equations 12 and 13.

The calculated values of R are compared with the experimental results in Fig. 6. The data and calculations are in good agreement except at the lowest value of total iron concentration, particularly at low oxygen partial pressures, where other

TABLE II Parameters used in the calculation of R at 1400° C. The values of A and ΔE are given for the equilibrium constants, $K = A \exp - \Delta E/(kT)$ for the processes indicated

Defect reaction	From [1]	From experimental data fit*		
	ΔE(eV)	A	ΔE	K ($T = 1400°$ C)
$Fe_{Mg}^{\cdot} + V_{Mg}'' \rightleftarrows (Fe_{Mg}^{\cdot}-V_{Mg}'')'$	−0.85	12	−0.69	1438
$Fe_{Mg}^{\cdot} + V_{Mg}'' \rightleftarrows (Fe_{Mg}^{\cdot}-O-V_{Mg}'')'$	−1.13	6	−0.92	3546
$Fe_{Mg}^{\cdot} + (Fe_{Mg}^{\cdot}-V_{Mg}'')' \rightleftarrows (Fe_{Mg}^{\cdot}-V_{Mg}''-Fe_{Mg}^{\cdot})^x$	−0.57	0.5	−0.46	12.2
$Fe_{Mg}^{\cdot} + (Fe_{Mg}^{\cdot}-O-V_{Mg}'')' \rightleftarrows (Fe_{Mg}^{\cdot}-O-V_{Mg}''-O-Fe_{Mg}^{\cdot})^x$	−1.07	0.5	−0.86	194.9
$2Fe_{Mg}^{x} + \frac{1}{2}O_2 \rightleftarrows 2Fe_{Mg}^{\cdot} + O_0^x + V_{Mg}''$	–	(3.7×10^{-5})†	−0.34	(3.9×10^{-4})†
Aluminium (and chromium):				
$Al_{Mg}^{\cdot} + V_{Mg}'' \rightleftarrows (Al_{Mg}^{\cdot}-V_{Mg}'')'$		12	−0.68‡	
$Al_{Mg}^{\cdot} + V_{Mg}'' \rightleftarrows (Al_{Mg}^{\cdot}-O-V_{Mg}'')'$		6	−0.86‡	
$Al_{Mg}^{\cdot} + (Al_{Mg}^{\cdot}-V_{Mg}'')' \rightleftarrows (Al_{Mg}^{\cdot}-V_{Mg}''-Al_{Mg}^{\cdot})^x$		0.5	−0.64‡	
$Al_{Mg}^{\cdot} + (Al_{Mg}^{\cdot}-O-V_{Mg}'')' \rightleftarrows (Al_{Mg}^{\cdot}-O-V_{Mg}''-O-Al_{Mg}^{\cdot})^x$		0.5	−0.82‡	
$Fe_{Mg}^{\cdot} + V_{Mg}'' + Al_{Mg}^{\cdot} \rightleftarrows (Fe_{Mg}^{\cdot}-V_{Mg}''-Al_{Mg}^{\cdot})^x$		1.0	−1.42§	
$Fe_{Mg}^{\cdot} + V_{Mg}'' + Al_{Mg}^{\cdot} \rightleftarrows (Fe_{Mg}^{\cdot}-O-V_{Mg}''-O-Al_{Mg}^{\cdot})^x$		1.0	−1.84§	

*$R_0 = ([Fe]_T = 7365) = 0.79$.
†If R_0 ($[Fe]_T = 7365$) = 0.80; $A = 4.3 \times 10^{-5}$ and $K = 4.6 \times 10^{-4}$; if R_0 ($[Fe]_T = 7365$) = 0.81, $A = 4.7 \times 10^{-5}$ and $K = 5.0 \times 10^{-4}$.
‡From [1].
§Estimates.

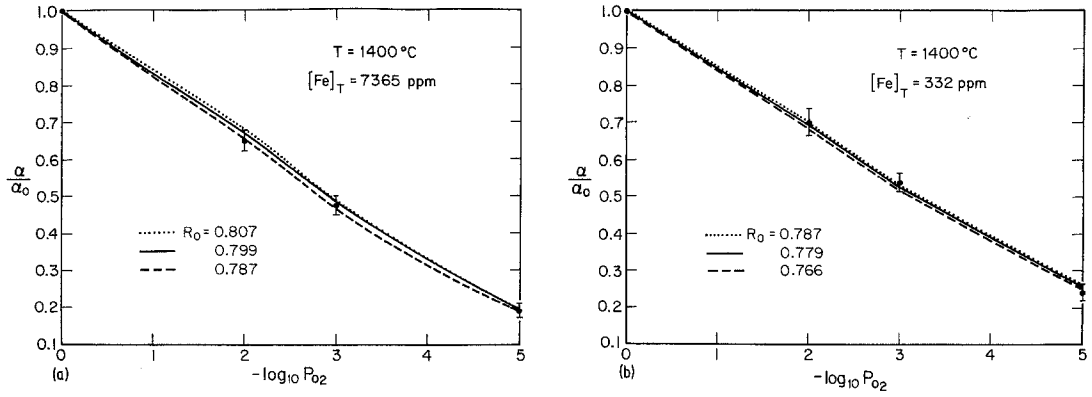

Figure 5 (a) Plot of α/α_0 versus $\log_{10} P_{O_2}$ at $T = 1400°$ C for $[Fe]_T = 7365$ ppm. The different values of R_0 correspond to different defect equilibrium parameters (Table II). (b) Plot of α/α_0 versus $\log_{10} P_{O_2}$ at $T = 1400°$ C and $[Fe]_T = 332$ ppm.

aliovalent solutes, principally Al^{3+} and Cr^{3+}, might have an influence even in these high purity crystals. Calculations indicate that Si^{4+} and charge compensating vacancies are completely associated and do not affect other equilibria even at high temperatures. Using the association energies for Al^{3+} calculated by Gourdin and Kingery [1], the influence of these impurities was added, with the constants shown in Table II as illustrated by the dashed lines in Fig. 6. This interaction between solutes is important at solute levels below a few hundred ppm and at low oxygen pressures.

The relevant data of Brynestad and Flood [2] are included in Fig. 6 and good continuity with the present work is found. This agreement provides further support for concluding that a model based on simple mass-action equilibria can account for the system behaviour over a wide range of oxygen partial pressures and iron contents.

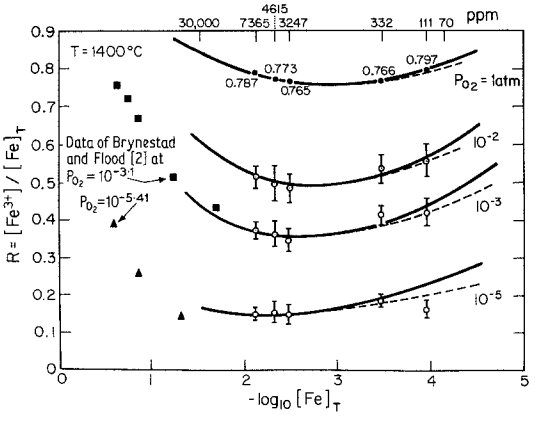

Figure 6 Plot of R as a function of $\log_{10} [Fe]_T$ at various partial pressures of oxygen, $T = 1400°$ C, and $R_0([Fe]_T = 7365) = 0.787$ (Table II).

Although this study was primarily limited to partial pressures greater than 10^{-5}, extrapolation to lower P_{O_2} is possible. When sample SP1–4300 was reduced at $P_{O_2} = 10^{-10}$, α/α_0 was found to be ~ 0.02, giving $R = 0.016$ in good agreement with the calculated value of 0.013. Data at high and low oxygen pressures at 1500° C are in good accord with interpretations of optical data by Blazey [21].

As illustrated in Fig. 7, the temperature dependence of the experimental values of R is in satisfactory accord with the constants derived at

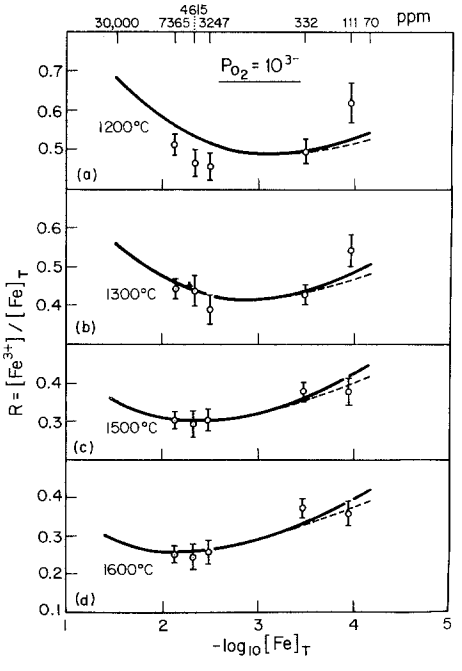

Figure 7 R as a function of temperature at $P_{O_2} = 10^{-3}$ for $R_0([Fe]_T = 7365) = 0.787$. Dashed lines show the effect of increasing the concentration of other aliovalent impurities to the levels for NOR1–122.

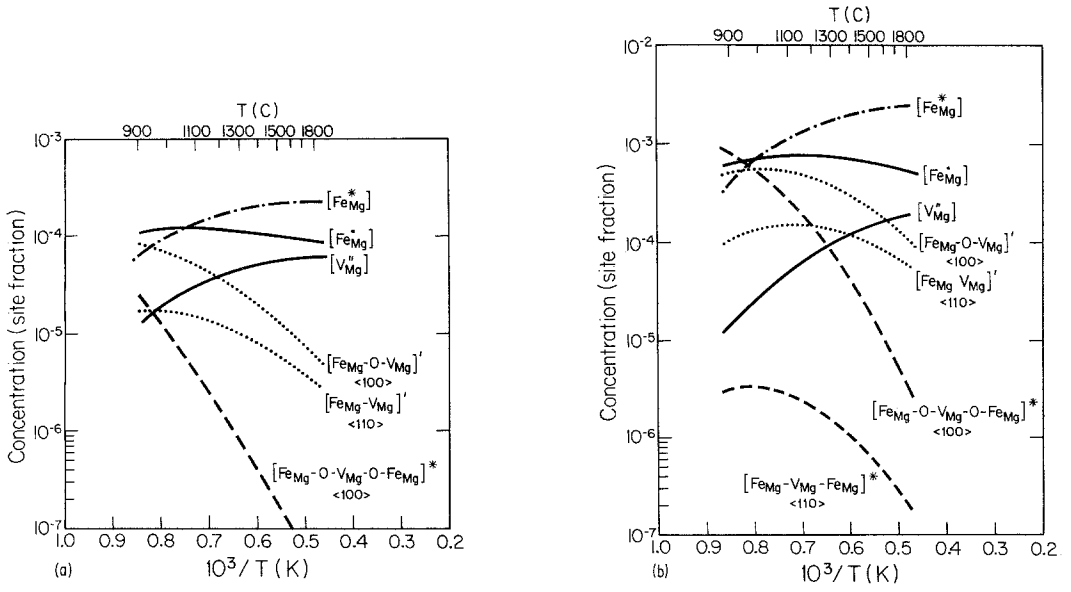

Figure 8 (a) Calculated defect concentrations for a composition corresponding to sample SP1–310 as a function of inverse temperature. (b) Calculated defect concentrations for a composition corresponding to sample SP1–2300 as a function of inverse temperature.

1400° C (Table II), for higher temperatures, i.e. 1500 and 1600° C, and at 1300° C except for the very low iron content sample. At 1200° C the agreement at both high and low iron contents is poor and efforts to achieve a better fit by modifying the constants used in the set of equations given in Table II were unsuccessful. The samples are well within the single-phase region at 1200° C, so precipitation is not likely. However, cluster formation of the kind described by Gourdin and Kingery [1] in which the Fe^{3+} moves to a tetrahedral site, or perhaps some unknown charge-compensating centre other than V''_{Mg} may affect the results. Our knowledge of lower temperature processes is inadequate to formulate testable conjectures. Using the equilibrium parameters collected in Table II, the concentrations of different defect species as a function of temperature were calculated and are shown in Fig. 8 for two compositions corresponding to our samples SP1–310 and SP1–2300. Readers will surely notice that the concentration, temperature and oxygen pressure dependence is more complex than is generally assumed in most interpretations of defect-dependent phenomena.

6. Conclusions

The experimental results of this study are in good accord with predictions based on a simple defect chemical model for the behaviour of iron solutes in magnesia. The quantitative agreement between calculated and measured values of the ratio $R = [Fe^{+3}]/[Fe]_T$ as a function of the total iron content ($[Fe]_T$), oxygen partial pressure (P_{O_2}) and temperature (T) (for $T \geqslant 1300°$ C) show that such models, predicated on mass-action relationships between various solute–vacancy associates, are capable of adequately describing the system behaviour over a range of several orders of magnitude in partial pressure and total iron content at moderately high temperatures. While it is clear that a spectrum of association and disassociation occurs as the conditions of $[Fe]_T$, P_{O_2} and T are changed, it cannot be inferred from the behaviour of R alone that those structures chosen are necessarily the correct ones. It is not possible, for example, to determine from the present data which trimer configuration dominates the defect structure at high iron contents and low temperatures or even if they exist at all in the form proposed. However, these results in conjunction with the shell-model calculations indicate that the model tested is highly plausible. Its success in describing the oxidation–reduction of iron indicates that it closely approximates the actual defect structure and that the calculated energies for the various vacancy–solute associates are reasonable.

In contrast, the poor agreement of experiment with calculations at 1200° C indicates that processes other than those specifically considered may

become important at lower temperatures. Further study of the kinetics of the oxidation–reduction process and the detection of polyatomic defect clusters seems to be indicated.

The conclusions drawn from this work may be briefly summarized as follows.

(1) The optical absorption at 4.3 eV (2880 Å) in the near ultraviolet provides a viable technique for determining the concentration of ferric ions present in solid solution in single-crystal MgO. A calibration curve may be established for specimens heat-treated in oxygen at 1400° C for which $R_0 = [Fe^{3+}]_0/[Fe]_T$ is approximately constant at 0.80 ± 0.01. Values for R determined with such a curve are found to be in good accord with previous work.

(2) A defect model consisting of trimer and dimer associates and characterized by mass-action equilibrium constants provides a satisfactory quantitative description of the behaviour of $R = [Fe^{3+}]/[Fe]_T$ as a function of $[Fe]_T$, P_{O_2} and T for $T \geqslant 1300°$ C. The parameters used to describe the interaction between the iron solutes and cation vacancies as well as the unassociated oxidation–reduction reaction are given in Table II.

(3) At temperatures of 1200° C or less, other defect–solute interactions not considered in the analysis may become important, effectively changing the amount of Fe^{3+} detected optically.

(4) The shell-model association energies calculated by Gourdin and Kingery [1] for $Fe_{Mg}^{\cdot}$ and V_{Mg}'' in MgO give a reasonable fit to experimental data when they are reduced by about 20%. This is in accord with prior comparisons with the experimental heat of solution [1].

(5) The use of numerical methods allows the complete calculation of the defect population implied by a set of equilibrium interactions and the requirements of mass, site and change balance. This population differs from that estimated on the basis of simple assumptions.

References

1. W. H. GOURDIN and W. D. KINGERY, *J. Mater. Sci.* **14** (1979) 2053.
2. J. BRYNESTAD and H. FLOOD, *Z. Electrochem.* **62** (1958) 953.
3. D. H. SPEIDEL, *J. Amer. Ceram. Soc.* **50** (1967) 243.
4. T. KATSURA and S. KIMURA, *Bull. Chem. Soc. Japan* **38** (1965) 1664.
5. J. C. K. SOONG and I. B. CUTLER, *J. Solid State Chem.* **3** (1971) 134.
6. P. M. VALET, W. PLUSCHKELL and H. J. ENGELL, *Arch. Eisenhüttensw.* **46** (1975) 383 (in German).
7. W. H. GOURDIN, Ph.D. Dissertation, MIT (1977).
8. P. REIJNEN, *Phillips Res. Reports* **23** (1968) 151.
9. B. H. A. CARNAHAN, H. A. LUTHER and J. O. WILKES, "Applied Numerical Methods", (Wiley, New York, 1969) p. 290.
10. H. WEBER, *Z. Physik* **130** (1951) 392.
11. R. W. DAVIDGE, *J. Mater. Sci.* **2** (1967) 339.
12. P. J. FICALORA and G. W. BRINDLEY, *J. Amer. Ceram. Soc.* **50** (1967) 662.
13. E. F. HARRIS and J. H. CRAWFORD, *Phys. Stat. Sol. (a)* **35** (1976) 667.
14. R. W. SOSHEA, A. J. DEKKER and J. P. STURTZ, *J. Phys. Chem. Solids* **5** (1958) 23.
15. W. T. PERIA, *Phys. Rev.* **112** (1958) 423.
16. R. L. HANSLER and W. G. SEGELKEN, *J. Phys. Chem. Solids* **13** (1960) 124.
17. Y. CHEN and W. A. SIBLEY, *Phys. Rev.* **154** (1967) 842.
18. J. P. MOLNAR and C. D. HARTMAN, *ibid* **79** (1950) 1015.
19. J. C. CHENG and J. C. KEMP, *Phys. Rev. B* **4** (1971) 2841.
20. J. A. TOSSELL, D. J. VAUGHAN and K. H. JOHNSON, *Nature Phys. Sci.* **244** (1973) 42.
21. K. W. BLAZEY, *J. Phys. Chem. Solids* **38** (1977) 671.

Received 15 August and accepted 2 October 1978.